Concepts
doi.org/10.1002/batt.202000221

Chemistry Europe
European Chemical Societies Publishing

Electrochemical Methods and Protocols for Characterization of Ceramic and Polymer Electrolytes for Rechargeable Batteries

Ramasubramonian Deivanayagam[a] and Reza Shahbazian-Yassar*[a]

Solid-state lithium batteries are widely believed to be the most feasible next-generation battery technology. New material candidates for solid electrolytes are typically screened using meticulous characterization methods and ranked using metrics such as ionic conductivity, transference number, decomposition voltage, and deposition/stripping overpotential. The determination of these metrics requires the use of a variety of electrochemical experiments, the details of which are scattered across existing literature and could be time-consuming for a beginner to locate. Here, we present a comprehensive overview of the electrochemical concepts, methods, and protocols adopted to characterize the polymer and ceramic electrolyte candidates for rechargeable batteries. This work facilitates the understanding of the key parameters involved in solid-state electrolyte characterization and in interpreting their data.

1. Introduction

Lithium-ion batteries have attracted a great attention within the materials research community over the last two decades. In pushing the limits of achievable energy densities and power densities, the contributions of the materials researchers played an important role during the last few decades. The community continues to pursue a target cost of $100/kWh for battery packs to make electric vehicles more affordable. To lower the cost of battery packs without having to compromise their energy, several next-generation battery technologies are currently under development by the community with separate efforts dedicated to electrodes and electrolytes. Solid-state batteries are a class of next-generation batteries that promise higher energy density and better safety by replacing the conventional liquid electrolyte and separator setup with a solid or a polymer electrolyte.

In solid-state batteries, the electrolyte plays an equally important role as the electrodes in determining the overall energy density. Ideally, a solid or a polymer electrolyte should possess a high ionic conductivity, a transference number close to unity, a high oxidative stability, a wide voltage window, minimal overpotentials when cycling with a metal anode, and a good stability in air and moisture.[1] Whenever a new solid or a polymer electrolyte candidate is proposed, these parameters need to be assessed first prior to testing their performance in full cells with a sample cathode and an anode.

To develop solid or polymer electrolytes that fulfill all the aforementioned requirements, there is a need for innovative solutions from researchers whose expertise span different research areas. In this circumstance, it is not uncommon for materials scientists and chemists to venture into electrochemistry and contribute to these vital research efforts. Although there exist several conceptual and tutorial articles in the literature that aid beginners in characterizing electrode materials,[2–6] there is a lack of such comprehensive tutorials in characterizing electrolyte candidates in general. This manuscript is aimed at reviewing the methods and protocols used to characterize electrolyte candidates for rechargeable batteries based on lithium, sodium, magnesium, aluminum, zinc, or calcium. Although the experiments are mostly similar across all metal-ion based rechargeable battery systems (Li, Na, Mg, Al, Ca, and Zn), we have chosen to describe them with Li-based systems in this article for the sake of simplicity.

2. Experimental Cell Setup

For the lab-scale testing of conventional rechargeable batteries, i.e., cells with a liquid electrolyte soaked in a separator, coin cells have been the most popular choice as the test vehicle. This is mainly due to their small size, speed and ease of cell assembly, and the ability to conduct electrochemical tests even with small quantities of materials.[2] Figure 1a shows the different components that comprise a coin cell setup. The coin cell set up can also be used for testing polymer electrolytes, simply by replacing the separator component with the desired polymer electrolyte membrane. However, if the polymer membranes are too thin (of the order of few tens of microns), the pressure provided by the coin cell's wave spring may not be sufficient, and would result in improper contact between the electrode and the electrolyte. This problem may be circumvented by using thicker spacers (0.2 or 0.5 mm thick spacers as opposed to the typical size of 0.1 mm), or by stacking multiple 0.1 mm spacers together. However, for the testing of ceramic electrolytes, coin cells may not be the most

[a] R. Deivanayagam, Prof. R. Shahbazian-Yassar
Department of Mechanical and Industrial Engineering
University of Illinois at Chicago
Chicago, IL 60607
E-mail: rsyassar@uic.edu

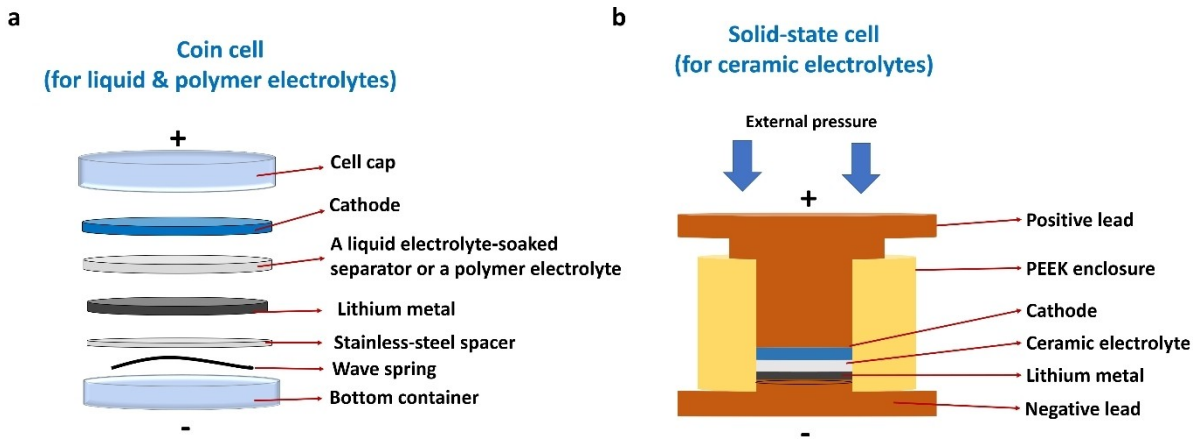

Figure 1. Cell Setups for Evaluating Liquid, Polymer and Ceramic Electrolytes. a) Schematic representing a coin cell that is typically used for testing liquid electrolytes and polymer electrolytes. b) Schematic of a solid-state cell used for testing ceramic solid electrolytes.

ideal choice due to the insufficient pressure even upon using multiple or thicker spacers. To ensure an intimate contact between the electrode and the electrolyte, a special cell setup may be needed that could be coupled to a mechanical fixture that provides external pressure. Figure 1b shows an example of a solid-state cell with a PEEK (polyether ether ketone) enclosure. However, for best results, it is recommended that ceramic electrolytes be tested using a solid-state cell coupled with a pressure jig fixture that provides at least 20 MPa pressure,[7] although it is not uncommon to come across higher pressures of up to 50 MPa[8] being applied to the solid state cell.

3. Conductivity via Blocking Electrode Setup

The ionic conductivity of a solid electrolyte is a crucial metric that influences the electrochemical performance of a solid-state battery.[9] The ionic conductivity is simply a measure of a material's tendency to conduct ions. Over the past decade, it has increasingly gained popularity as the most defining parameter used in ranking battery electrolyte candidates.[9] This is especially true in the cases of polymer and inorganic solid electrolytes, as there are a wide variety of polymer hosts and crystal structures available with varying ion conduction mechanisms. Typically, the ionic conductivity of an electrolyte is measured using a technique called the electrochemical impedance spectroscopy (EIS), also known as AC impedance spectroscopy. However, it is important to note that the value measured using this technique includes that of all mobile ions regardless of their charge. In this technique, a potential with a small amplitude is applied to the desired cell set up using a potentiostat while sweeping the frequency across several orders of magnitude (1 MHz–10 mHz). Then, the cell's overall impedance response is recorded in terms of the frequency and represented in the form of an impedance spectrum. There are two ways commonly used to represent the impedance spectrum: (i) the Nyquist plot, which plots the real and imaginary parts of the impedance, and (ii) the Bode plot, which shows the magnitude changes as a function of the frequency. Unlike the Nyquist plot, Bode plot has the advantage of showing the frequency information and may be useful for identifying the frequency at which a phenomenon of interest occurs. This representation may be useful for the analysis of filters and transistors. However, for the case of lithium-ion batteries, Nyquist plot is more commonly used since it helps in identifying circuit elements which may aid in explaining the behavior of the system as a whole. Figure 2a represents a

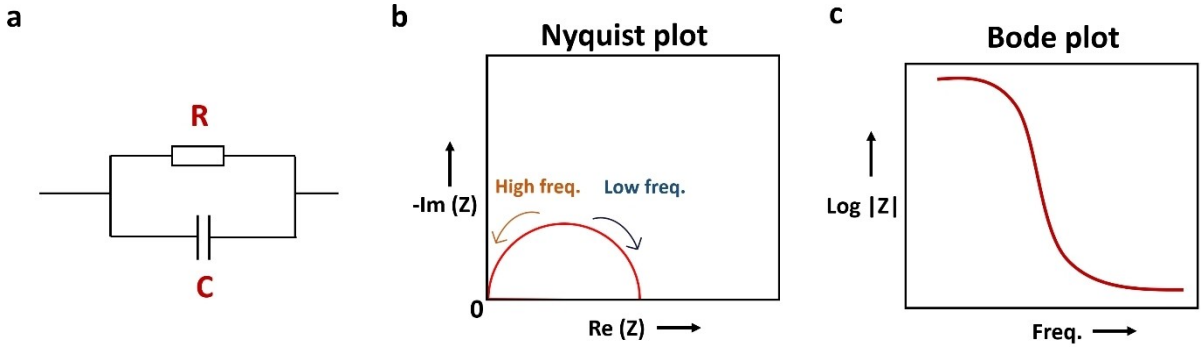

Figure 2. Representation of an Electrochemical Impedance Spectrum. a) A simple equivalent circuit with one resistor and one capacitor, b) Nyquist plot corresponding to the circuit in (a), c) Bode plot corresponding to the equivalent circuit in (a)

simple equivalent circuit with a resistor and a capacitor. Figure 2b-c represent the Nyquist plot and Bode plot corresponding to this circuit, respectively.

For measuring the ionic conductivity of an electrolyte, a symmetric cell is assembled with the electrolyte material sandwiched between two 'blocking' electrodes. A 'blocking' electrode refers to an electrode in which faradaic reactions are not possible and therefore, the cell built with such electrodes behaves as a capacitor. Using a blocking electrode simplifies the measurement by excluding the possibility of any electron transfer reaction and helps in measuring the bulk resistance of the electrolyte. Stainless steel, gold, and platinum are typically used as blocking electrodes. On the other hand, a 'non-blocking' electrode refers to an electrode where only faradaic reactions occur, and the charge transfer resistance is negligible (E.g. lithium metal). A schematic of a blocking electrode setup is shown in Figure 3a. This electrode setup can be represented by the equivalent circuit as shown in Figure 3b, where the bulk resistance of the electrolyte, R_b, lies in parallel with the geometric capacitance C_b. The value C_b, represents the geometric capacitance and has its origins in the charges present on the electrodes irrespective of the presence of the electrolyte. This geometric capacitance does not appear in liquid electrolyte systems since it lies outside the frequency range studied.[10] Figure 3c shows the typical Nyquist plot for a symmetric non-blocking electrode configuration. Ideally, the double-layer capacitance in the circuit would appear as a straight line. However, in practical scenarios, non-ideal capacitances are observed,[10] as indicated in Figure 3c. In an ideal blocking electrode setup, two main elements contribute to the overall cell impedance. They are (i) bulk of the electrolyte – with its own resistive and capacitive components, and (ii) double-layers that get capacitively charged upon polarization. For this circuit, the total impedance is given by Equation (1):

$$Z = Z_b + Z_D \tag{1}$$

where Z_b and Z_D denote the bulk and double-layer contributions of the impedances, respectively.

The bulk impedance Z_b, arising from a combination of a resistor (R_b) and capacitor (C_b) in parallel, can be represented as in Equations (2) and (3):

$$\frac{1}{Z_b} = \frac{1}{R_b} + \frac{1}{1/i\omega C_b} \tag{2}$$

$$Z_b = \frac{R_b}{1 + i\omega C_b R_b} \tag{3}$$

The double layer impedance Z_D can be represented as in Equation (4)

$$Z_D = \frac{1}{i\omega C_D} \tag{4}$$

where C_D denoted the double layer capacitance. Although the term "double layer" is commonly used to refer to the capacitive phenomena occurring at the electrode-electrolyte interface, strictly speaking, this phenomenon is distinct from the space charge layer that is observed in solid/solid interfaces. The former is specific to electrolyte (or) solution media that have mobile anions and cations, whereas the latter is specific to solid-solid interfaces and are not necessarily caused by anionic/cationic migrations.

As far as ionic conductivity is concerned, the bulk resistance, R_b is the quantity of our interest. At high frequencies ($\omega \to \infty$), the bulk impedance tends to become zero. At low frequencies ($\omega \to 0$), the denominator in Equation (3) becomes unity and therefore, the bulk impedance arises solely from the bulk resistance, R_b. Thus, when cell's overall impedance response is represented in the form of a Nyquist plot which plots the real part of the impedance against its imaginary component (Figure 1c), the x-intercept in the low-frequency region gives the value of the bulk resistance, R_b. The conductivity of an electrolyte is calculated using this bulk resistance and the geometry of the electrolyte/electrode interface using Equation (5)

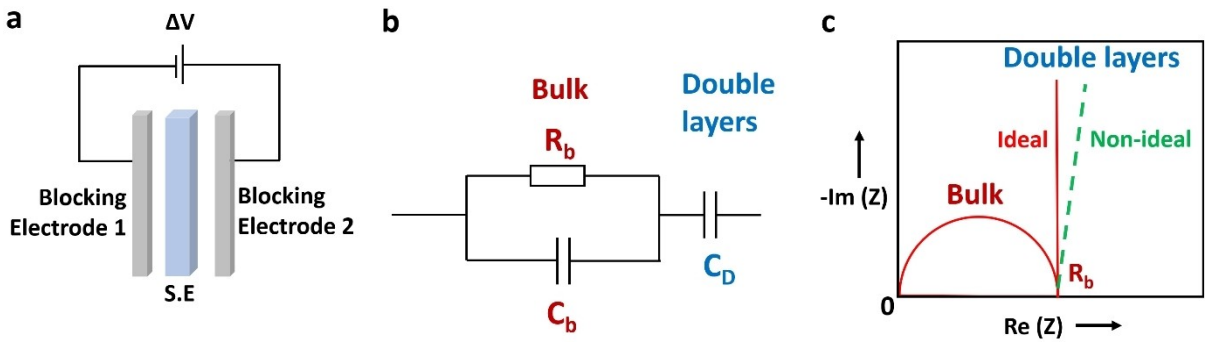

Figure 3. Measuring Ionic Conductivity using a Blocking Electrode Setup. a) Schematic of a symmetric cell with a solid electrolyte (S.E) in a blocking electrode configuration used for measuring conductivity. b) A typical equivalent circuit used to represent a cell with ideally blocking electrodes. c) A typical Nyquist plot of such an equivalent circuit with the regions indicating the contribution from bulk and double layers.

$$\sigma = \frac{l}{R_b A} \tag{5}$$

where l and A denote the thickness and surface area of the electrolyte layer respectively, and R_b denotes the resistance obtained from the Nyquist plot.[11]

4. Transference Number via DC Polarization Tests

Transference number is used to quantify the fraction of ionic transport and the cationic/anionic contribution to the overall ionic conductivity. Even if an electrolyte were to possess an excellent ionic conductivity, it is the transference number that determines the number of useful cations that can be shuttled between the electrodes in a rechargeable metal-ion battery. Despite being such an insightful metric, in most reports on electrolytes, it is not always calculated or accounted for. It is extremely crucial to measure cationic transference number to get a reliable quantification of an electrolyte's ionic conductivity.

One of the most common methods to determine the transference number involves a combination of Wagner's DC polarization test[12] and AC impedance spectroscopy, more commonly known as the Bruce-Vincent method.[13] During the DC polarization test, a symmetric two-electrode cell in a non-blocking configuration is polarized by applying a small step potential (say, 0.01 V) and the resulting potentiostatic current is monitored as a function of time. The cell's impedances are recorded before and after the polarization. The polarization causes a concentration gradient to develop across the length of the electrolyte as depicted in Figure 4. The interfacial resistance is noted at the steady state and used in the derivation below to estimate the transference number of the electrolyte.

Before a symmetric cell with an electrolyte (either an inorganic solid electrolyte, or a LiX salt dispersed in a solvent/polymer) is polarized, the concentrations of cationic and ionic species are approximately the same on either side of the electrolyte layer, as represented in Figure 4a. However, when a constant potential is applied, the electrolyte's cations (Li^+) are forced to accumulate on the negatively polarized end, while the anions are forced to the other end. While the motion of Li^+ ions is driven by both migration and diffusion in the same direction, the directions of motion of X^- anions by these processes are conflicted. Eventually, a steady state is reached where a definitive gradient of the ionic species develops across the entire length of the electrolyte, as shown in Figure 4b. The continuous current that flows in the circuit at this stage is termed as steady-state current.

The derivation of the equation for transference number through Bruce-Vincent method is a fairly simple one, as illustrated by Lacey[14] as follows: The transference number is given by the ratio of the steady state current (I_{ss}) to the initial current (I_0) [Eq. (6)]:

$$t_+ = \frac{I_{SS}}{I_0} \tag{6}$$

Here, the initial current is given by Equation (7)

$$I_0 = \frac{\sigma A}{l}\Delta V \tag{7}$$

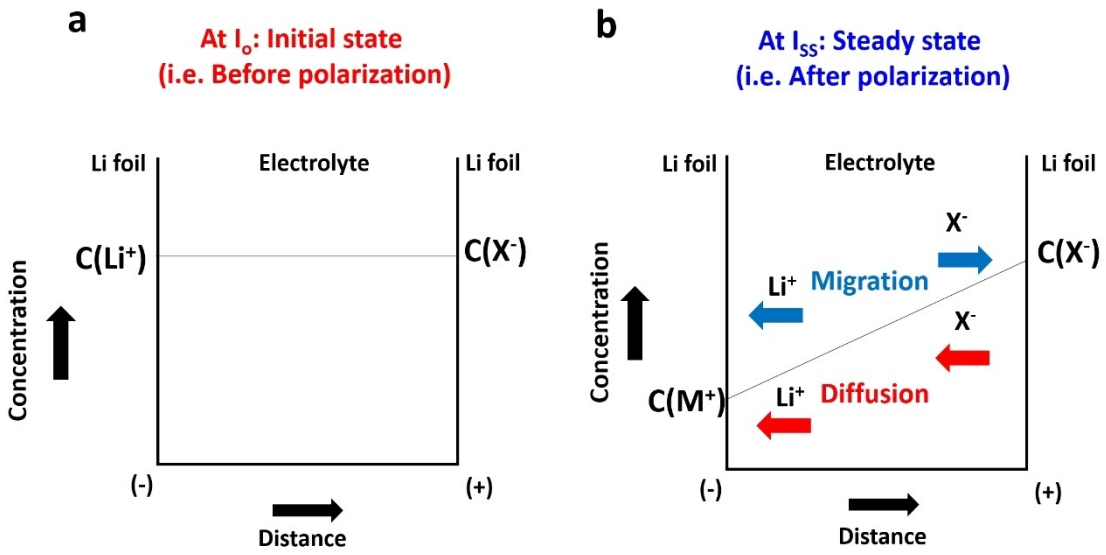

Figure 4. Schematic of Initial and Steady States in DC Polarization. Schematic depicting the concentrations of the ionic species in a symmetric Li|Li cell across the length of the electrolyte with a sample LiX salt a) at the initial state, b) after a polarization potential is applied and the steady state is attained. The blue and red arrows indicate the directions of ion movement due to migration and diffusion, respectively.

where σ, A, l, ΔV denote the conductivity, area of the electrode, thickness of the electrolyte membrane, and the DC polarization potential, respectively. The steady state current is given by Equation (8)

$$I_{SS} = \frac{t_+ \sigma A}{l} \Delta V \tag{8}$$

For practical systems, the interfacial resistances must also be accounted for. Therefore, the initial and steady-state currents will become Equations (9) and (10):

$$I_0 = \frac{1}{\left(\frac{l}{\sigma A}\right) + R_{\text{int},0}} \Delta V \tag{9}$$

$$I_{SS} = \frac{1}{\left(\frac{l}{t_+ \sigma A}\right) + R_{\text{int,SS}}} \Delta V \tag{10}$$

where, $R_{\text{int},0}$ and $R_{\text{int,SS}}$ denote the initial and steady-state interfacial resistances, respectively. Rearranging the terms in Equation (9), we get an expression for $\frac{\sigma A}{l}$ as follows [Eq. (11)]:

$$\frac{\sigma A}{l} = \frac{I_o}{\Delta V - I_o R_{int,0}} \tag{11}$$

Substituting the value of $\frac{\sigma A}{l}$ from Equation (11) in (10), i.e., expression for steady-state current, and rearranging the terms, we get an expression for transference number as follows [Eq. (12)]:

$$t_+ = \frac{I_{SS}\ (\Delta V - I_0 R_{\text{int},0})}{I_0 (\Delta V - I_{SS} R_{\text{int,SS}})} \tag{12}$$

We do note that the determination of the initial current, I_0 is not straightforward and is limited by the response time of the instrument. If the initial current cannot be determined with certainty, the initial current (I_0) can be substituted with I_Ω calculated using Ohm's law as follows [Eq. (13)]:[15]

$$I_\Omega = \frac{\Delta V}{R_{\text{b},0} + R_{\text{int},0}} \tag{13}$$

where $R_{\text{b},0}$ denotes the bulk resistance. Alternatively, Hiller et al.[16] proposed an approach wherein a new term for the electrolyte resistance of the equilibrium electrolyte, R_{el}, can be defined as follows [Eq. (14)]:

$$R_{\text{el}} = \frac{l}{\sigma_{\text{eq}} A} = \frac{\Delta V - I_0 R_{\text{int},0}}{I_0} \tag{14}$$

where σ_{eq} denotes the total equilibrium conductivity of the homogeneous binary electrolyte (LiX). The transference number relation in Equation (12) can then be written as [Eq. (15)]:

$$t_+ = \frac{I_{SS}\ R_{\text{el}}}{(\Delta V - I_{SS} R_{\text{int,SS}})} \tag{15}$$

Sample data of the impedance measurements and the chronoamperometry plot obtained from the DC polarization test are shown in Figure 5a-c. Numerical calculations provide an illustration of estimating the transference number from the data in Figure 5.

Initial current, $I_0 = 0.055$ μA,
Steady state current, $I_{SS} = 0.032$ μA,
Polarization potential, $\Delta V = 0.010$ V
Initial interfacial resistance, $R_{\text{int},0} = 2200\ \Omega$
Steady-state interfacial resistance, $R_{\text{int,SS}} = 3027\ \Omega$
Using the relation for transference number in Equation (12),

$$t_+ = \frac{0.032^{*}10^{-6}\ (0.010 - 0.055^{*}10^{-6}{}^{*}2200)}{0.055^{*}10^{-6}\ (0.010 - 0.032^{*}10^{-6}{}^{*}3027)}$$

$$t_+ = 0.58^{*}\frac{(0.009879)}{(0.009903)}$$

$$t_+ = 0.57$$

The closer the value of t_+ is to unity, the higher the fraction of transported ions that consists solely of cations. The value of t_+ in liquid and polymer electrolytes in the literature have been reported to be in a range of between 0.10–0.50, whereas for solid ceramic electrolytes, it can reach as high as unity.[17–19]

In addition, the electronic conductivity can be determined by polarizing a symmetric cell with the electrolyte sandwiched between two blocking electrodes. Here, in the chronoamperometry plot, the current tends to immediately drop to a negligible (or) residual value, i_r. The electronic conductivity can be calculated using the relation [Eq. (16)]:

$$\mathrm{Y} = \frac{i_r l}{VA} \tag{16}$$

where l and A denote the thickness and surface area of the electrolyte layer respectively, and V denotes the polarization applied.[20] For an ideal solid electrolyte, the value of electronic conductivity should be between 10^{-10} and 10^{-12} S cm^{-1}, which is several orders of magnitude lower than the typical ionic conductivity values observed in solid electrolytes.[21,22]

Although the estimation of transference numbers through Bruce-Vincent technique seems straightforward, this method relies on one key assumption.[19,23] This method is based on the dilute solution theory, which uses the electrostatic potential, a quantity that is well defined only in infinite dilution.[24] Corrections to this technique using the concentrated solution theory requires the measurement of additional properties such as salt activity coefficients or the electrophoretic mobilities.[19]

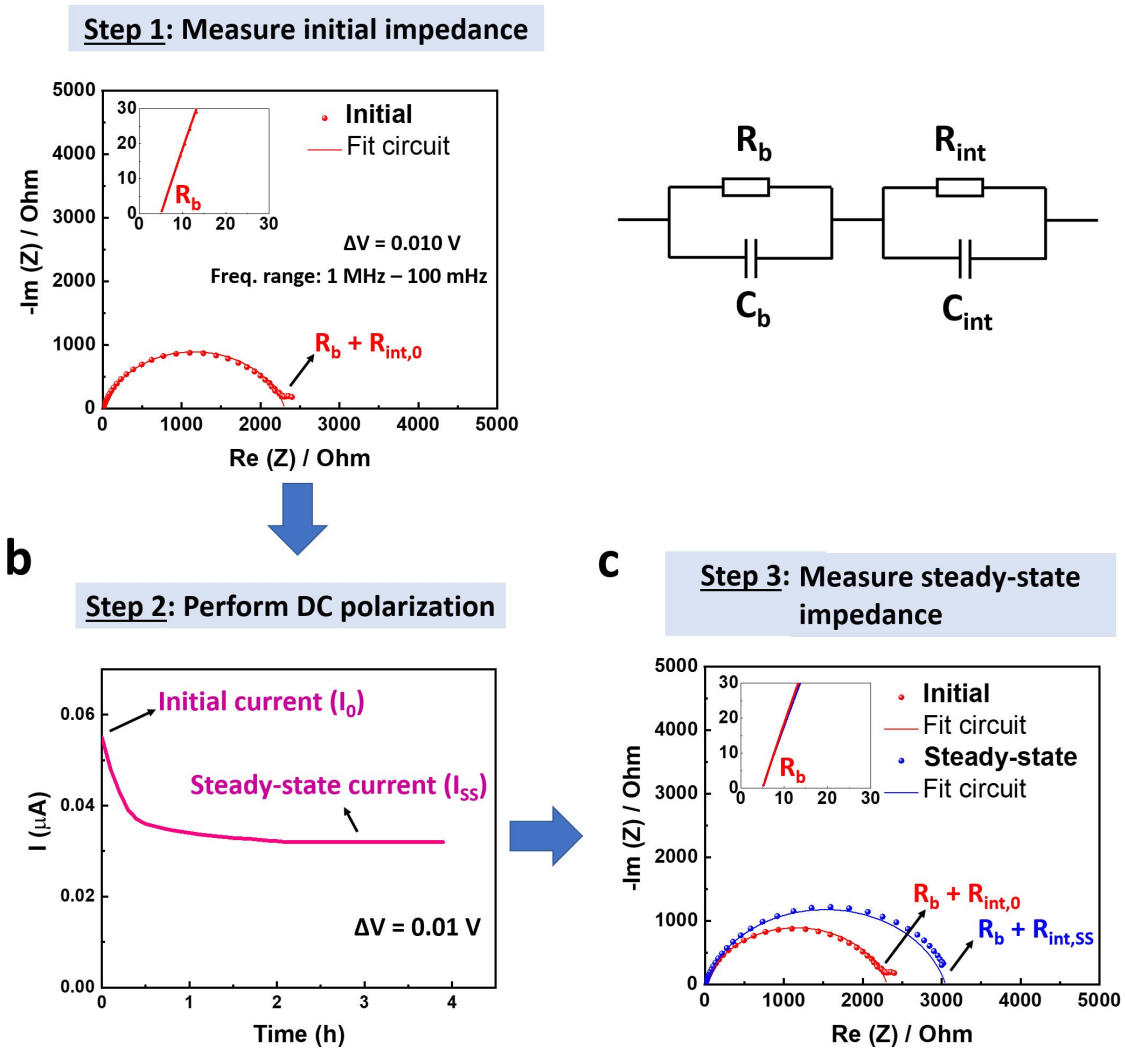

Figure 5. Sample Data for the Estimation of the Transference Number. a) Nyquist plot showing the initial impedance of the symmetric cell. The circuit on the right shows the typical equivalent circuit used to model a symmetrical cell with non-blocking electrodes. b) Chronoamperometry plot obtained after the DC polarization test showing the steady-state condition. c) Nyquist plot showing both the initial and steady-state impedances. Insets in (a) and (c) show the bulk resistance R_b.

5. Anodic Stability via Linear Sweep Voltammetry

The anodic (or) oxidative stability of an electrolyte determines the effective 'voltage window', i.e., the highest voltage up to which a cell can be cycled without letting the electrolyte to decompose. This metric is used to determine the maximum voltage of the battery cathode that can be cycled without any side reactions or deterioration of the electrolyte. This decomposition voltage of the electrolyte could be determined by performing a Linear Sweep Voltammetry (LSV) with a simple Li|SS two-electrode cell for Li^+ conducting electrolyte. While Li can be used as the reference electrode in lithium-ion two-electrode cells, Mg metal would be a poor reference electrode for evaluating magnesium-ion electrolytes. This is because, Mg metal, unlike Li, forms a passivation film on its surface which blocks divalent cation migration.[25] Therefore, its use as a reference electrode is applicable to only to a few electrolytes (namely, Grignard reagent-based electrolytes) which can inhibit the growth of the passivation layer.

Upon cell assembly, the voltage is scanned from OCV to a high positive voltage V_2, say 5.0 V. The onset of a decomposition phenomenon will be accompanied by a steep increase in the current during a voltage sweep in the high-voltage region. Figure 6 shows a typical LSV plot where the asymmetric cell was scanned up to 5.0 V. Here, the onset of decomposition occurs at 2.5 V, and then after a gradual increase, the current starts to increase exponentially after 4.0 V. The onset can be more accurately determined from the x-intercept of the tangent of the first step of the current increase.

The electrochemical window is established by setting an arbitrary current density threshold, say 0.1 mA cm^{-2}. However, the onset of the current is influenced by various factors such as reaction volume, voltage scan rate, temperature, and the current collector material.[26–28] The use of a two-dimensional electrode-electrolyte interface (such as a coin-cell) often leads

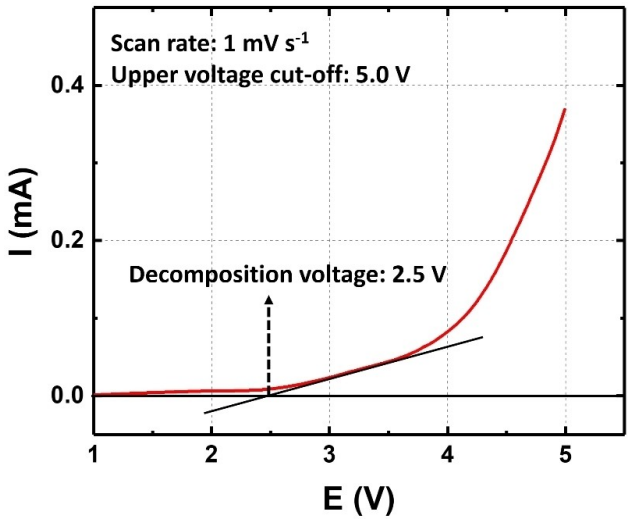

Figure 6. A Sample Linear Sweep Voltammogram. A sample linear sweep voltammetry plot depicting the voltage at which the electrolyte starts to degrade.

to overestimation of the onset potential. In liquid electrolyte systems, this can be circumvented by the use of a 3-electrode cell setup wherein electrode rods are immersed in the liquid. However, this may not be feasible for ceramic or polymer electrolytes. Similarly, larger scan rates also lead to an overestimation of the onset potential. Typically, a value of 0.1 V s^{-1} or lower is chosen for an accurate estimation of the onset potential. Higher test temperatures also facilitate a thermodynamically driven decomposition, and lead to lower onset potentials. For instance, a $LiBH_4$ solid electrolyte exhibits an onset potential of 2.04 V vs. Li+/Li at 60 °C, and 1.96 V vs. Li^+/Li at 120 °C.[26]

For conventional ether-based electrolytes for Li^+ systems, it is quite common to find that their voltage stabilities lie below 4.0 V vs. Li^+/Li. It may be possible to tune the stabilities of certain electrolytes at 4.5 V, but only at high concentrations.[29] As for Mg^{2+} ion systems, it has been a challenge to develop electrolytes that are stable for more than 3.0 V vs. Mg^{2+}/Mg^0. If the decomposition of the electrolyte occurs at a low voltage (for e.g., $<$2.5 V), then it may not be able to even access the intercalation voltage of many potential Mg-ion intercalating cathode materials.[30] Most of the earlier electrolytes developed for Mg batteries, incorporated organic solvents which possessed a low decomposition voltage of $<$2.4 V. Therefore, the experimental screening of the cathode materials had been severely limited by the stability of the electrolytes. Consequently, the electrolyte's oxidative stability serves as the limiting factor for achieving high energy densities. This is especially true in case of Mg-ion batteries because, only a handful of reported electrolytes have been reported to be stable at voltages up to, and higher than 3.0 V. Grignard reagents, the electrolytes that were first reported to reversibly deposit magnesium, had a low voltage stability of ~1.5 V. Use of optimal constituents and cosolvents such as triglyme increased the decomposition voltage to 2.2 V.[31] Despite targeted efforts, the best oxidative stability that could be realized experimentally for a Mg-ion battery electrolyte is 3.8 V vs. Mg^{2+}/Mg^0.

6. Cyclic Voltammetry to Ascertain Plating and Stripping of Metal Ions

Cyclic voltammetry (CV) could be considered as an extended version of an LSV in the sense that the voltage is scanned *back* after scanning across a predefined range from V_1 to V_2.[32–34] The current response is recorded from sweeps of both directions. A comparison of the shape and current magnitudes provides information on the reversibility of the reaction. This experiment is typically conducted prior to ascertaining the long-term cyclability of an electrolyte candidate in a full-cell setup. Figures 7a-c show the snapshots of a typical cyclic voltammograms and the corresponding cell processes within the cell. For half cells with lithium metal as the electrode, the cell OCV is the same as the equilibrium potential of the positive electrode, i.e. the stainless steel (in this experimental setup). This is because, in a two-electrode cell setup, the Li metal also acts as the reference electrode and the potential of Li metal is 0 V vs. Li^+/Li. For the example illustrated, the OCV value is close to 3.0 V vs. Li^+/Li. When the voltage of the working electrode ($E_{W.E}$), i.e., the stainless-steel disc, is scanned to lower values, there is no reaction observed until it reaches 0.0 V vs. Li^+/Li. When the voltage is scanned further lower, the current begins to increase indicating the onset of Li depletion from the Li foil and plating on the stainless-steel surface. This depletion will continue as long as the voltage is lowered, indicated by a linear increase in the current (Figure 7b). This is because the Li foil serves as a practically unlimited source of Li^+ ions. Once a voltage reaches the preset lower voltage limit (and the current reaches a corresponding maximum, I_{max}), it begins to scan back. Up to 0.0 V vs. Li^+/Li, the current mostly retraces the original path. Beyond 0.0 V vs. Li^+/Li, the current starts to increase in the positive reaction. This indicates the onset of stripping (or) the removal of plated Li from the stainless-steel disc. However, unlike the linear increase seen in the cathodic scan, the current peaks at a value $<=I_{max}$, and then drops to a negligible value (Figure 7c). This is an indication of the limited Li available to strip from the stainless-steel disc. In addition to the qualitative analysis, it is also possible to quantify the reversibility of the Li plating/stripping through cyclic voltammogram by comparing the Coulombic efficiencies (C.E). As far as voltammetric experiments are concerned, it is advantageous to measure the charge rather than the current.[35] The integration of the peaks provides direct information about the amount of charge transferred during any electrochemical reaction. Since Coulombic efficiencies are based on the charge transferred, the reversibility of the plating/stripping process can be quantified by measuring and comparing the integral of the voltammetric peaks.

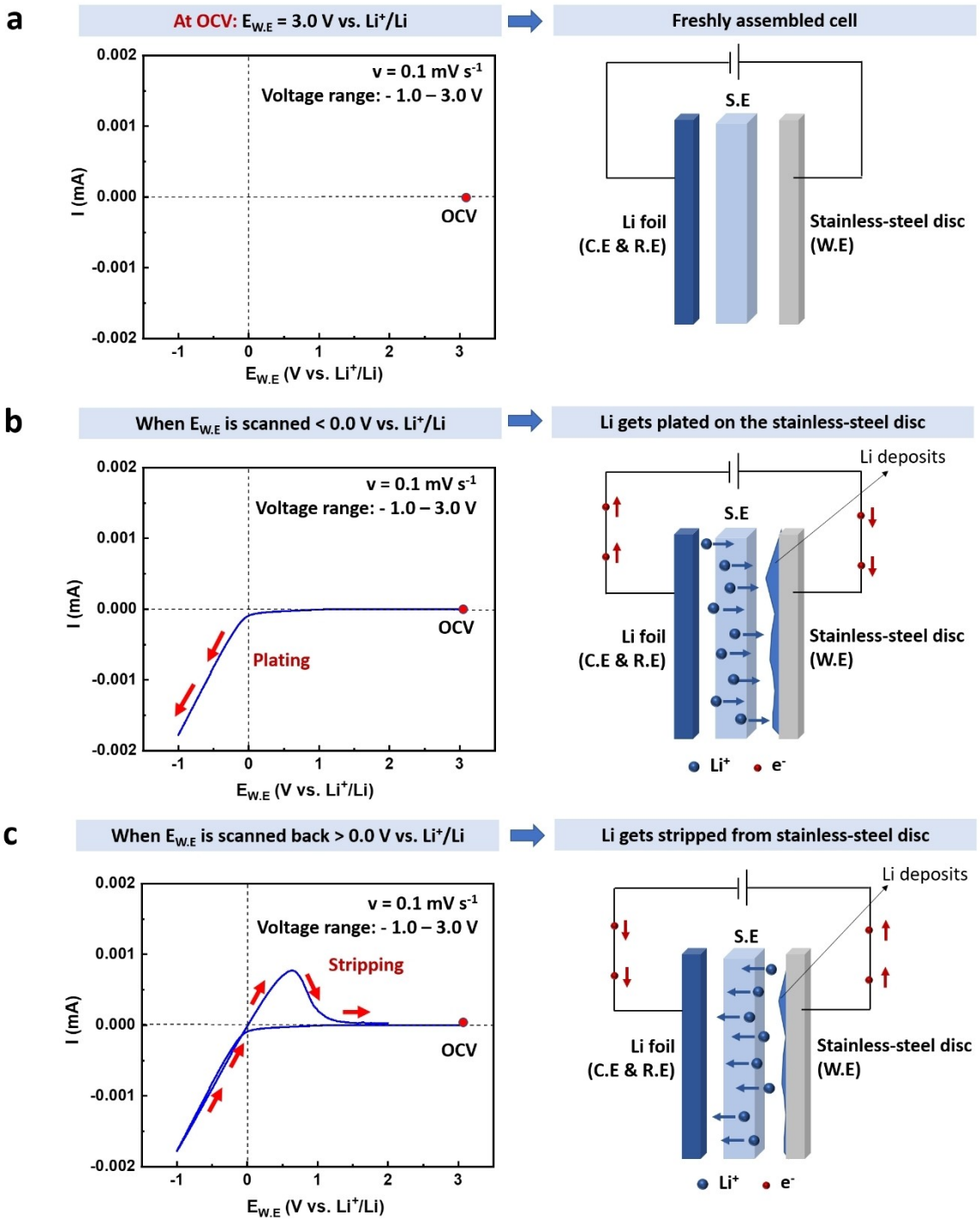

Figure 7. Cyclic Voltammogram of a Li vs. Stainless-steel Two-electrode Cell with a Solid Electrolyte (S.E). Snapshots of a typical cyclic voltammogram of a Li vs. stainless-steel cell and their respective representations of the phenomena inside the cell a) at OCV, b) when the voltage is scanned below 0.0 V vs. Li+/Li, c) when the voltage is scanned back above 0.0 V vs. Li+/Li.

7. Galvanostatic Cycling to Measure Overpotentials

Although the occurrence of peaks in cyclic voltammogram and a steady current in DC polarization test indicate cationic transport in the electrolyte, galvanostatic cycling tests must be carried out to provide clear evidence of the reversible nature of the metal's plating/stripping from the foil. The overpotential values observed in such galvanostatic cycling tests are a measure of the ease of deposition/stripping from the foil surface and therefore, help in determining the electrolyte's suitability in metal batteries.

For measuring overpotentials, symmetric cells with non-blocking electrodes are used. If the objective is to estimate the

Li plating/stripping overpotentials of an electrolyte, a symmetric cell of the electrolyte sandwiched between two Li foils is used. Figure 8a shows the schematic of a symmetric Li–Li cell. A constant current is applied to the cell for a certain time interval T_c, and the potential is obtained a function of time. If the potential is stable for as long as the current is applied, it means that the processes of Li depletion on one electrode and Li plating on the other electrode is concurrent. Figure 8b shows the first discharge step, and the corresponding measurement of overpotential. At the end of one discharge step, the current is reversed and continued for the same interval of time. This will evoke a corresponding reversal in the sign of the potential, indicating that the plating/stripping processes that occurred in the discharge step is reversed (Figure 8c). This discharge and charge step is continued for several hours (in hundreds) to

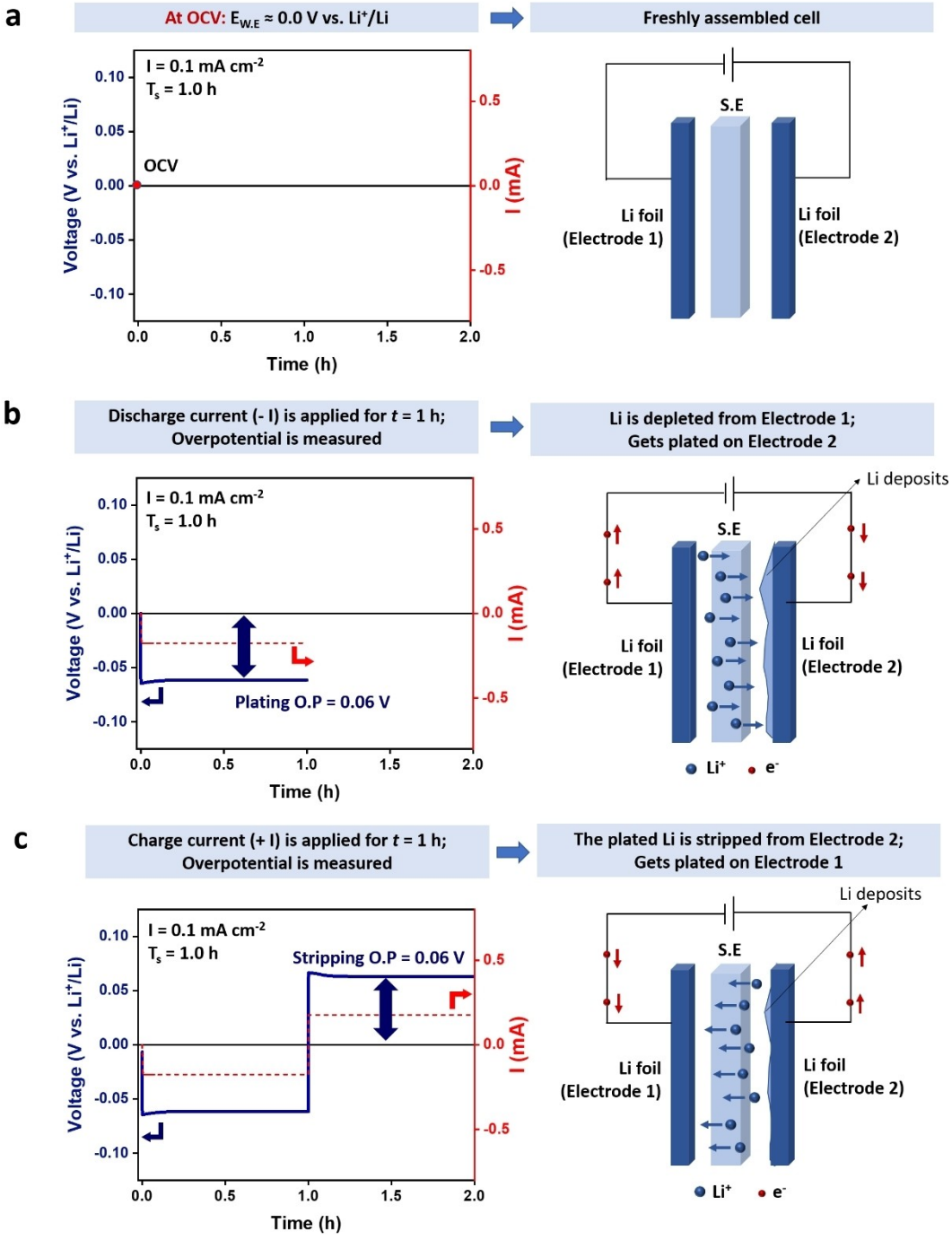

Figure 8. Galvanostatic Cycling of a Symmetric Li vs. Li Two-electrode Cell with a Solid Electrolyte (S.E). a) Voltage profile showing the OCV of a symmetric Li–Li cell, and a schematic of the cell before applying any current. b) First discharge step of the cell showing the current applied and the overpotential measured. Schematic shows the depletion of Li on Electrode 1 and plating of Li on Electrode 2. c) First charge step of the cell showing the reverse current applied and the corresponding potential measured. Schematic shows the stripping of plated Li from Electrode 2.

determine the overall stability and efficiency of the deposition/stripping process.

It has generally been observed that electrolytes with high ionic conductivities exhibit low deposition/stripping overpotentials. Low overpotentials are also indicative of low interfacial resistance between the electrodes and the electrolyte.[9] The typical ambient-temperature plating/stripping overpotentials reported in the literature for solid polymer electrolytes lie within the range of 0.05–0.5 V vs. Li^+/Li for current densities of 0.05–0.2 mA cm^{-2},[36–39] and are much lower i.e., <0.1 V vs. Li^+/Li for liquid electrolyte candidates at current densities of 1.0 mA cm^{-2}. An increasing overpotential increasing with the number of cycles is often an indication of a thick and a growing interfacial layer and could ultimately be detrimental for further cycling. In full-cell tests, such a behavior could be attributed to both the electrolyte and the electrode material, and therefore, additional tests may be necessary to pinpoint the source of the capacity fade. However, in a symmetric cell test, an increase in overpotential can be solely attributed to the electrolyte, provided that the surfaces of Li foils are free of the oxide layer. Therefore, galvanostatic cycling tests with symmetric cells provide a simpler way to characterize an electrolyte's ability to plate/strip metal ions. Moreover, compared to the electrochemical testing with full cells (e.g., with an intercalation cathode and an anode), the galvanostatic cycling with symmetric cells (Li | Li) serve as a quicker method to evaluate whether the electrolyte could support reversible cycling. This is because, when an intercalation cathode is cycled at a rate of C/10 (typical rate used for evaluating new materials), it would take about 20 hours to obtain one full cycle. However, when a symmetrical cell with Li is cycled, we should be able to obtain data for several cycles within a few hours, depending on the experiment settings applied. Typically, a test protocol of 1 hour of stripping and 1 hour of plating is considered a single "cycle" in the symmetric cell tests. With this setting, it is possible to obtain 5 reversible cycles within 10 hours (the time frame for obtaining 1 cycle an intercalation cathode).

While the voltage profiles in Figure 8 show the ideal scenario, the profiles in practice may not look as smooth. In a symmetric cell, the half cycle begins with the nucleation and since the nucleation is always a kinetically slow process, it occurs as a peak with shallow slope in the beginning of the voltage profile.[40,41] As soon as the nucleation has begun at a fairly large number of sites, the deposition begins, the kinetics transition to a faster phase, and the profile tends to become flatter. At the end of the half cycle, when the cell polarization reaches a maximum, bulk dissolution (kinetically slow process) starts to occur, which once again appears as a peak towards the end of the half cycle. Understandably, for systems with poorer performance, a peak occurs at the early stage of the voltage profile half-cycles and has a steeper slope.[40] On the other hand, for electrolytes that possess low interfacial resistance, the peak is usually less prominent and only occurs during the second half of the half-cycle.

8. Conclusions

We have summarized the electrochemical methods that are used to determine the performance metrics for ceramic or polymer electrolyte candidates for rechargeable batteries. Each of the quantities measured through these techniques gives an insight into the ease of ionic conduction between the two electrodes within a cell, and therefore helps in pre-evaluating the electrochemical performance of the full cell. For instance, the voltammetry experiments shed light on the reversibility and the cyclable voltage window, thereby helping us screen the potential anodes and cathodes suitable for coupling with the solid electrolyte. However, it must also be noted that there are limitations and caveats associated with conducting these experiments with two-electrode cells. To exclude the effects of the side reactions or passivation on the reference electrode, the cyclic and linear sweep voltammetry experiments must be carried out with three electrode setups utilizing a distinct counter and reference electrode when possible. The galvanostatic cycling with symmetric cells helps in understanding the reversibility of metal ion plating/stripping over several cycles. The deposition/stripping overpotentials are increasingly being used to characterize solid electrolytes. In addition to these metrics, the transference number is also an important metric to rank solid electrolytes and is routinely ignored or not reported in manuscripts that detail new electrolyte candidates. Given how important it is in ascertaining the movement of fraction of 'useful' cations, this test must be carried out in order to convincingly claim that an electrolyte is functioning. However, the measurement of transference number through the conventional Bruce-Vincent method may not always yield the most accurate results owing to the assumptions involved. Alternatively, one could make use of spectroscopic techniques such as solid state, pulsed field gradient – nuclear magnetic resonance (PFG-NMR) spectroscopy to estimate the transference numbers. It is indeed quite common to supplement these electrochemical tests with other sophisticated studies such as Fourier-transform infrared spectroscopy (FTIR), nuclear magnetic resonance (NMR) spectroscopy, and molecular dynamics simulations. However, the electrochemical methods described here provide a quicker and more intuitive data about the electrolyte's conduction behavior. We believe that this Concept article will aid beginners and experts from other fields to get a quick start into experimental research of battery electrolytes.

Acknowledgements

The authors acknowledge the financial support from National Science Foundation (NSF) Award no. CBET-1805938.

Conflict of Interest

The authors declare no conflict of interest.

Keywords: batteries · solid electrolytes · solid-state batteries · polymer electrolytes · electrochemistry

[1] J. Muldoon, C. B. Bucur, A. G. Oliver, T. Sugimoto, M. Matsui, H. S. Kim, G. D. Allred, J. Zajicek, Y. Kotani, *Energy Environ. Sci.* **2012**, *5*, 5941.
[2] E. Talaie, P. Bonnick, X. Sun, Q. Pang, X. Liang, L. F. Nazar, *Chem. Mater.* **2017**, *29*, 90.
[3] X. Yang, A. L. Rogach, *Adv. Energy Mater.* **2019**, *1900747*, 1.
[4] T. S. Mathis, N. Kurra, X. Wang, D. Pinto, P. Simon, *Adv. Energy Mater.* **2019**, *1902007*, 1.
[5] Y. Cao, M. Li, J. Lu, J. Liu, K. Amine, *Nat. Nanotechnol.* **2019**, *14*, 200.
[6] B. Wu, Y. Yang, D. Liu, C. Niu, M. Gross, L. Seymour, H. Lee, P. M. L. Le, T. D. Vo, Z. D. Deng, E. J. Dufek, M. S. Whittingham, J. Liu, J. Xiao, *J. Electrochem. Soc.* **2020**, *166*, A4141.
[7] X. Zhang, Q. J. Wang, K. L. Harrison, S. A. Roberts, S. J. Harris, *Cell Reports Phys. Sci.* **2020**, *1*, 100012.
[8] S. Randau, D. A. Weber, O. Kötz, R. Koerver, P. Braun, A. Weber, E. Ivers-Tiffée, T. Adermann, J. Kulisch, W. G. Zeier, F. H. Richter, J. Janek, *Nat. Energy* **2020**, *5*, 259.
[9] P. Oh, H. Lee, S. Park, H. Cha, J. Kim, J. Cho, *Adv. Energy Mater.* **2020**, *10*, 1.
[10] J. Mindemark, M. J. Lacey, T. Bowden, D. Brandell, *Prog. Polym. Sci.* **2018**, *81*, 114.
[11] X. Qian, N. Gu, Z. Cheng, X. Yang, E. Wang, S. Dong, *J. Solid State Electrochem.* **2001**, *6*, 8.
[12] J. B. Wagner, C. Wagner, *J. Chem. Phys.* **1957**, *26*, 1597.
[13] J. Evans, C. A. Vincent, P. G. Bruce, *Polymer* **1987**, *28*, 2324.
[14] M. J. Lacey, *Transport and Transference Number in Battery Electrolytes*, **2019** http://lacey.se/science/transference/.
[15] D. M. Pesko, Z. Feng, S. Sawhney, J. Newman, V. Srinivasan, N. P. Balsara, *J. Electrochem. Soc.* **2018**, *165*, A3186.
[16] M. M. Hiller, M. Joost, H. J. Gores, S. Passerini, H. D. Wiemhöfer, *Electrochim. Acta* **2013**, *114*, 21.
[17] S. Zugmann, M. Fleischmann, M. Amereller, R. M. Gschwind, H. D. Wiemhöfer, H. J. Gores, *Electrochim. Acta* **2011**, *56*, 3926.
[18] K. M. Diederichsen, E. J. McShane, B. D. McCloskey, *ACS Energy Lett.* **2017**, *2*, 2563.
[19] K. A. Dwelle, A. P. Willard, *J. Chem. Phys.* **2020**, *152*, 1.
[20] F. Wu, N. Chen, R. Chen, Q. Zhu, G. Tan, L. Li, *Adv. Sci.* **2016**, *3*, 1500306.
[21] F. Han, A. S. Westover, J. Yue, X. Fan, F. Wang, M. Chi, D. N. Leonard, N. J. Dudney, H. Wang, C. Wang, *Nat. Energy* **2019**, *4*, 187.
[22] L.-P. Wang, F. Klein, Z. Zhao-Karger, J. Chable, T. Braun, A. R. Schür, C.-R. Wang, Y.-G. Guo, M. Fichtner, *ChemSusChem* **2019**.
[23] M. D. Galluzzo, J. A. Maslyn, D. B. Shah, N. P. Balsara, *J. Chem. Phys.* **2019**, *151*.
[24] N. P. Balsara, J. Newman, *J. Electrochem. Soc.* **2015**, *162*, A2720.
[25] R. Dugas, J. D. Forero-Saboya, A. Ponrouch, *Chem. Mater.* **2019**.
[26] R. Asakura, L. Duchêne, R. S. Kühnel, A. Remhof, H. Hagemann, C. Battaglia, *ACS Appl. Mater. Interfaces* **2019**, *2*, 6924.
[27] G. F. Dewald, S. Ohno, M. A. Kraft, R. Koerver, P. Till, N. M. Vargas-Barbosa, J. Janek, W. G. Zeier, *Chem. Mater.* **2019**, *31*, 8328.
[28] T. Swamy, X. Chen, Y. M. Chiang, *Chem. Mater.* **2019**, *31*, 707.
[29] X. Ren, L. Zou, S. Jiao, D. Mei, M. H. Engelhard, Q. Li, H. Lee, C. Niu, B. D. Adams, C. Wang, J. Liu, J. G. Zhang, W. Xu, *ACS Energy Lett.* **2019**, *4*, 896.
[30] R. Deivanayagam, B. J. Ingram, R. Shahbazian-Yassar, *Energy Storage Mater.* **2019**, *21*, 136.
[31] D. Aurbach, H. Gizbar, A. Schechter, O. Chusid, H. E. Gottlieb, Y. Gofer, I. Goldberg, *J. Electrochem. Soc.* **2002**, *149*, A115.
[32] N. Elgrishi, K. J. Rountree, B. D. McCarthy, E. S. Rountree, T. T. Eisenhart, J. L. Dempsey, *J. Chem. Educ.* **2018**, *95*, 197.
[33] E. M. Espinoza, J. A. Clark, J. Soliman, J. B. Derr, M. Morales, V. I. Vullev, *J. Electrochem. Soc.* **2019**, *166*, H3175.
[34] G. A. Mabbott, *J. Chem. Educ.* **1983**, *60*, 697.
[35] J. C. Myland, K. B. Oldham, C. G. Zoski, *J. Electroanal. Chem.* **1985**, *182*, 221.
[36] L. Porcarelli, C. Gerbaldi, F. Bella, J. R. Nair, *Sci. Rep.* **2016**, *6*, 19892.
[37] H. Wang, D. Lin, Y. Liu, Y. Li, Y. Cui, *Sci. Adv.* **2017**, *3*, 1.
[38] Y. Liu, D. Lin, Z. Liang, J. Zhao, K. Yan, Y. Cui, *Nat. Commun.* **2016**, *7*, 10992.
[39] R. Deivanayagam, M. Cheng, M. Wang, V. Vasudevan, T. Foroozan, N. V. Medhekar, R. Shahbazian-Yassar, *ACS Appl. Mater. Interfaces* **2019**, *22*.
[40] K. N. Wood, E. Kazyak, A. F. Chadwick, K. H. Chen, J. G. Zhang, K. Thornton, N. P. Dasgupta, *ACS Cent. Sci.* **2016**, *2*, 790.
[41] A. J. Sanchez, E. Kazyak, Y. Chen, K. H. Chen, E. R. Pattison, N. P. Dasgupta, *ACS Energy Lett.* **2020**, *5*, 994.

Manuscript received: September 16, 2020
Revised manuscript received: December 3, 2020
Accepted manuscript online: December 10, 2020
Version of record online: January 14, 2021